A 1-D 2-phase control-oriented mass transfer model of PEM fuel cells

Raphaël Gass
Aix-Marseille Univ, LIS, Marseille, France
Univ. of Franche-Comte, FEMTO-ST, FCLAB
raphael.gass@lis-lab.fr

Zhongliang Li
Univ. of Franche-Comte, institut FEMTO-ST, FCLAB
Belfort, France
zhongliang.li@univ-fcomte.fr

***Abstract*—Controlling optimally the operating parameters of proton exchange membrane fuel cells (PEMFCs) is promising to improve its performance. A control-oriented model is often needed to favour the control design. In this paper, a 1-D 2-phase control-oriented mass transfer model is developed. The objective of developing such a model is to reveal fuel cell internal states in real-time. A nodal method is proposed to discretize the model spatial dimension and enable the real-time model implementation. Moreover, the model parameter identification for the developed model is presented to achieve reliable model calibration. The model is tested and analyzed in dynamic operating conditions and its potential applications are discussed in this paper.**

***Index Terms*—PEM fuel cells, control, mass transfer, two phase flow, model reduction**

I. Introduction

Proton exchange membrane fuel cell (PEMFC) technologies are rapidly developing in recent years to decarbonize heavy transports with the use of hydrogen [1]. However, the automated control of these systems is generally based on dynamic 0-dimensional (0D) models that consider fuel stacks as black boxes, sacrificing accuracy for simplicity and short computation times [2]. Other models in the literature are generally 2-D or 3-D, which offer accuracy, but require a lot of computing time and power [3], and therefore cannot be used for embedded systems. Models based on artificial intelligence (AI) are also being developed, which offer a combination of accuracy and speed, but are ineffective when it comes to extrapolating operating conditions that are too different from those for which they were trained [4], which bring risk.

To real-time acquire relevant information for control, a 1-D 2-phase model is developed. To achieve precise control, real-time knowledge of the spatial distribution of internal states within the fuel stack is necessary. These states encompass the concentrations of reactants and products, the proportion of liquid or dissolved water in the membrane, and the flow of matter throughout the stack. These variables primarily evolve in the thickness direction of the stack, which is why a 1-D model was selected.

This work has been supported by French National Research Agency via project DEAL (Grant no. ANR-20-CE05-0016-01), the EIPHI Graduate School (contract ANR-17-EURE-0002) and the Region Bourgogne Franche-Comté.

Additionally, to ensure precision, it was deemed necessary to analyze each physical quantity as a function of time, making the model dynamic. Furthermore, the condensation of water vapour within the stack is important to consider as flooding must be closely monitored. As a result, the model accounts for two states of water molecules: vapour and liquid, making it a 2-phase model.

For the model resolution, a nodal method is employed as it offers a simple and fast approach for solving a problem that cannot be solved analytically [5]. The choice of using 9 nodes was made to keep the number of nodes to a minimum, thereby reducing the calculation time, while still accounting for all the phenomena of matter transport within the cell. In addition, the model parameter identification is also designed in a prudent manner.

The remaining paper is organized as follows: the model is firstly described in Section II. In this part, we take the example of 2-phase water transfer to explain the whole mass transfer model. Following that, model resolution and model parameter identification are respectively presented in Section III and IV. The results, including parameter identification and model test, are provided in Section V. The application of the proposed model is also discussed in the same section. The paper is finally concluded in Section VI.

II. Mass transfer modelling of PEMFC

A. 1-D mass transfer model description

In this section, the 1-D 2-phase water transfer model will be described by providing the involved governing equations. For the other matters, i.e., hydrogen and oxygen, the governing equations are not provided in this paper since the nature is similar to these for water transfer.

B. 2-phase water transfer model

1) Water transfer in membrane: The water that flows in membrane is in the form of dissolved water and it becomes vapour water when water passes to catalyst layer (CL).

The governing equations for water transfer in membrane is summarized as follows,

$$\begin{cases} \frac{\rho_{mem}}{M_{eq}} \frac{\partial \lambda_{mem}}{\partial t} = -\boldsymbol{\nabla} \cdot \boldsymbol{J_{mem}}, & membrane \\ \frac{\rho_{mem} \varepsilon_{mc}}{M_{eq}} \frac{\partial \lambda_{cl}}{\partial t} = -\boldsymbol{\nabla} \cdot \boldsymbol{J_{mem}} + S_{sorp} + S_{prod}, & CL \end{cases} \tag{1}$$

where ρ_{mem}, λ_{mem}, $\boldsymbol{J_{mem}}$, M_{eq}, λ_{cl} are membrane density, water content, water flow rate, equivalent molar mass and water content in catalyst layer. S_{sorp} and S_{prod} are respectively water sorption rate and production rate. ε_{mc} is ionomer volume fraction.

Water flow rate $\boldsymbol{J_{mem}}$ is composed by two terms corresponding to electro-osmotic drag and water diffusion effects, as

$$\boldsymbol{J_{mem}} = \frac{2.5}{22}\frac{i_{fc}}{F}\lambda\ \boldsymbol{\imath} - \frac{\rho_{mem}}{M_{eq}} D\left(\lambda\right)\boldsymbol{\nabla\lambda} \tag{2}$$

The boundary condition is

$$\boldsymbol{J_{mem}^{cl,mem}} = \mathbf{0}, \text{at the ionomer border} \tag{3}$$

2) Water transfer modelling in CL and GDL: Through porous CL and gas diffusion layer (GDL), two-phase water transfer is involved. The liquid water transfer is dominated by capillary flow and modelled as follows:

$$\rho_{H_2O}\varepsilon\frac{\partial s}{\partial t} = -\boldsymbol{\nabla}\cdot\boldsymbol{J_l} + M_{H_2O}S_{vl} \tag{4a}$$

where s is liquid water saturation. ρ_{H_2O} and M_{H_2O} are water density and molar mass. $\boldsymbol{J_{cap}}$ is capillary flow rate. S_{vl} is water phase transfer rate of condensation and evaporation. ε is the porosity.

$$\boldsymbol{J_l} = -D_{cap}\left(s,\varepsilon\right)\boldsymbol{\nabla}s \tag{4b}$$

The boundary conditions at the interface of catalyst layer and membrane and that between GDL and GC are respectively

$$\begin{cases} \boldsymbol{J_l^{cl,mem}} = \mathbf{0}, \text{at the ionomer border} \\ \boldsymbol{J_l^{gdl,gc}} = \boldsymbol{J_{l,codi}^{gdl,gc}}(s, C_{l,gc}) \end{cases} \tag{4c}$$

where $\boldsymbol{J_{l,codi}^{gdl,gc}}$ is the convective-diffusive flow rate at the GDL and gas channel (GC) boundary. The vapour water transfer is dominated by concentration gradients and modelled as follows:

$$\varepsilon\frac{\partial}{\partial t}\left(\left[1-\mathrm{s}\right]C_v\right) = -\boldsymbol{\nabla}\cdot\boldsymbol{J_{v,dif}} - S_{sorp} - S_{vl} \tag{5}$$

where C_v is the water vapour concentration. $\boldsymbol{J_{v,dif}}$ is the water vapour flow rate.

The conditions at the two boundaries are respectively

$$\begin{cases} \boldsymbol{J_v^{cl,mem}} = \mathbf{0}, \text{at the ionomer border} \\ \boldsymbol{J_v^{gdl,gc}} = \boldsymbol{J_{v,codi}^{gdl,gc}}(C_v, C_{v,gc}) \end{cases} \tag{6}$$

where $\boldsymbol{J_{v,codi}^{gdl,gc}}$ is the convective-diffusive flow rate of water vapour.

3) Mass transfer in GC and auxiliary fluid subsystems: The water transfer in GC is modelled in a simple manner and the water concentrations of liquid water and water vapour are calculated as follows:

$$\frac{\mathrm{d}C_{l,gc}}{\mathrm{dt}} = \frac{J_{l,in}^{gc} - J_{l,out}^{gc}}{L_{gc}} + \frac{J_l^{gdl,gc}}{H_{gc}} \tag{7}$$

$$\frac{\mathrm{d}C_{v,gc}}{\mathrm{dt}} = \frac{J_{v,in}^{gc} - J_{v,out}^{gc}}{L_{gc}} + \frac{J_v^{gdl,gc}}{H_{gc}} \tag{8}$$

where $J_{l,in}^{gc}$, $J_{v,in}^{gc}$, $J_{l,out}^{gc}$, $J_{v,out}^{gc}$ are respectively liquid and vapour flow rates at inlet and outlet of GC. The values of these variables are provided by the auxiliary models whose details can be found in [2]

C. Voltage modelling

The overall output fuel cell voltage U_{cell} is modelled in the following way:

$$U_{cell} = U_{eq} - \eta_c - i_{fc}\left[R_p + R_e\right] \tag{9}$$

where U_{eq} is equilibrium potential, η_c is the over-potential containing both activation and concentration losses, R_p and R_e are respectively proton and electron resistances.

The equilibrium potential is

$$\begin{aligned} U_{eq} = {} & E^0 - 8.5\cdot10^{-4}\left[T_{fc} - 298.15\right] + \\ & \frac{RT_{fc}}{2F}\left[\ln\left(\frac{RT_{fc}C_{H_2^{cl}}}{P_{\text{ref}}}\right) + \frac{1}{2}\ln\left(\frac{RT_{fc}C_{O_2^{cl}}}{P_{\text{ref}}}\right)\right] \end{aligned} \tag{10}$$

where T_{fc} is fuel cell temperature, $C_{H_2}^{cl}$ and $C_{O_2}^{cl}$ are the hydrogen and oxygen concentration at the catalyst layers of anode and cathode. P_{ref} is the reference pressure which equals to the operation pressure. R and F are respectively gas constant and Faraday constant.

The over-potential is calculated as follows:

$$\eta_c = \frac{RT_{fc}}{\alpha_c F} ln\left(\frac{i_{fc}+i_n}{i_{0,c}^{ref}}\left[\frac{C_{O_2}^{ref}}{C_{O_2^{cl}}}\right]^{\kappa_c}\right) \tag{11}$$

where α_c is charge-transfer coefficient, i_n is internal current density, $C_{O_2}^{ref}$ is the reference concentration, $i_{0,c}^{ref}$ is the reference exchange current at cathode side, κ_c is over-potential correction exponent.

The proton resistance correlated to membrane characteristics is often more important than electron resistance to quantify Ohmic loss. The membrane resistance is modelled as

$$R_{mem} = \begin{cases} \frac{H_{mem}}{\left[0.5139\cdot\lambda - 0.326\right]\exp\left(1268\left[\frac{1}{303.15} - \frac{1}{T_{fc}}\right]\right)}, & \text{if } \lambda \geq 1 \\ \frac{H_{mem}}{0.1879\exp\left(1268\left[\frac{1}{303.15} - \frac{1}{T_{fc}}\right]\right)}, & \text{if } \lambda < 1 \end{cases} \tag{12}$$

III. Nodal resolution of the model

Nodal modelling involves dividing the spatial dimension into discrete nodes, with each node representing a specific volume. In between two neighboured nodes, all quantities are assumed to be homogeneous. In this work, a fuel cell is divided into 9 distinct zones with 9 nodes as shown in Fig. 1.

It is noted that we include an additional node at each GDL, specifically at the boundary with the bipolar plate. These additional nodes, labelled as nodes 2 and 8 in Figure 1, are required to account for the material discontinuity between the GDL and the GC.

Once the model is discretized in space using 9 nodes, the model form is transformed to regular differential equation concerning the time variables on the nodes. For the transformed regular differential equations, the 'BDF' (Backward Differentiation Formula) method, available in the '`solve_ivp`'

function of Python's scipy.integrate module, has been utilized [6]. This method offers several advantages. For instance, stiff problems can be effectively handled. Moreover, variable step size which results in a significant reduction in computation time.

IV. Parameter identification of the proposed model

In the proposed mass transfer model, two types of model parameters need to be identified.

- Accessible parameters: parameters that can be measured or accessed. These parameters include the active area, the membrane thicknesses, the GDL thicknesses, the GC thicknesses, the GC width and the GC total length.
- Fuel cell dependent parameters: parameters that need to be calibrated according to the experimental data.

The fuel cell dependent parameters are summarized in table I. Bounds of these parameters have also been fixed to limit the search for each parameter. The table indicates the voltage loss associated with each parameter: activation losses (Act.), ohmic losses (Ohm.), or mass transfer losses (Mass). It also specifies whether the impact is moderate (+) or significant (++).

The vertical order in which the parameters are listed in table I has been carefully chosen. The authors propose a methodology to effectively complete the manual calibration of the fuel cell dependent parameters.

TABLE I: Fuel cell dependent parameters

Variable	Range	Voltage loss relevance		
		Active loss	Ohmic loss	Mass transport loss
$i_{0,ca,ref}$	$[0.001, 500]$	++		
$C_{O_2,ref}$	$[3.39, 40.89]$	++		
κ_c	$[0.01, 100]$	++		
α_c	$[0.1, 0.5]$	++		
ε_{mc}	$[0.15, 0.4]$		++	
κ_c	$[0, 100]$	+	++	+

V. Results and discussion

In this section, the parameters of the proposed model are firstly identified to fit the experimental polarization curve data. The model will then be tested using a step change current profile. The evolutions of various parameters through the fuel cell layers are illustrated and analyzed. After that, the potential use of the proposed model is discussed. In this work, the detailed accessible fuel cell parameters can be found in [7].

A. Model calibration and validation

As discussed in IV, fuel cell dependent parameters are identified to fit the model output to experimental data. The polarization curve data are used to identify the parameters listed in Table I. The output of fitted model output and the experimental data are shown in Fig. 2. It can be seen that the static voltage calculated using the proposed model fit well the experimental data. However, it should be pointed out that the most accurate method of model identifying and validating a physical fuel cell model is to compare the spatial distribution of internal states predicted by the model with the real data. Limited by the capacity of available in-situ in-operando measurements, the physical model is only tested at macroscopic level via polarization curve in this work. Efforts are made to avoid over-fitting problems by configuring reasonable parameter ranges.

B. Analysis variable evolutions in transition periods

The fitted model is tested in a dynamic condition in which the the current profile is shown in Fig. 3.

The water content at different positions of membrane are shown in Fig. 4. The water content increases with current increase in general. In the transition time (280 s), it can be seen nevertheless that the water content at the anode side decreases during a short time. This can be linked to the electro-osmatic drag effect.

The water concentration rate and liquid water saturation are shown respectively in Fig. 5 and 6. It can be observed that the water concentration is generally lower than the water saturation threshold. During the current transition period at 280 s, the water concentration at node 6 (cathode electrode) exceeds the threshold and liquid water appears at the cathode CL and GDL.

The hydrogen and oxygen concentration rates are shown respectively in Fig. 7 and 8. The gas concentration is generally lowered at the CLs when current increases. This reduced concentration results in the concentration loss in the fuel cell output voltage.

The voltage behaviour in the process is finally illustrated in Fig. 9.

C. Model applications

As the evolution of different mass concentrations can be calculated through the proposed model in dynamic processes, it is therefore possible to build a link between different operating parameters and the fuel cell internal states, such as water saturation and membrane water concentration rate. Thus, the operating parameters can be optimized explicitly.

VI. Conclusion

In this paper, we have proposed a 1-D 2-phase control-oriented mass transfer model for PEMFC. Following a comparative study, it was concluded that the proposed model is relevant for describing the internal states of the stack and for a real-time implementation. The model can be applied to estimate the internal states water and reacts and link the evolution of these states with fuel cell operation. It is therefore promising to use the proposed model for optimal control design.

In the following work, it is still necessary to test the model with experimental data obtained in varied operating conditions to enhance the model generalization capability. It is also worthwhile to exploit the developed model within the control framework.

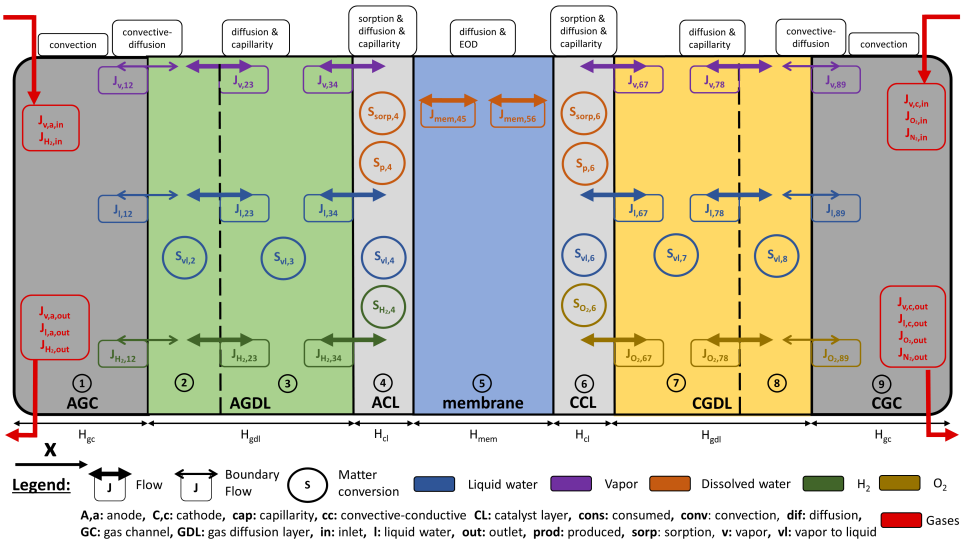

Fig. 1: Model resolution via notal method

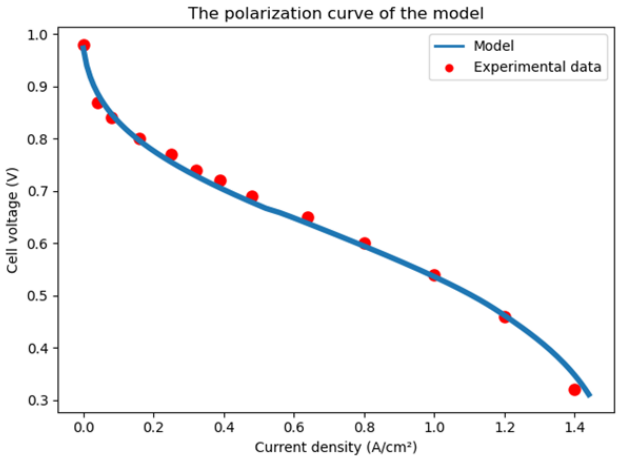

Fig. 2: Fitted polarization curve versus experimental data

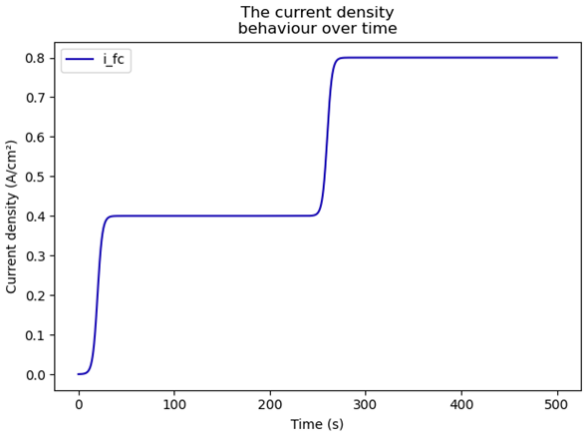

Fig. 3: Input current versus time

REFERENCES

[1] K. Jiao, J. Xuan, Q. Du, Z. Bao, B. Xie, B. Wang, Y. Zhao, L. Fan, H. Wang, Z. Hou, S. Huo, N. P. Brandon, Y. Yin, and M. D. Guiver, "Designing the next generation of proton-exchange membrane fuel cells," *Nature*, vol. 595, no. 7867, pp. 361–369, Jul. 2021.

[2] J. T. Pukrushpan, H. Peng, and A. G. Stefanopoulou, "Control-Oriented Modeling and Analysis for Automotive Fuel Cell Systems," *Journal of Dynamic Systems, Measurement, and Control*, vol. 126, no. 1, pp. 14–25, Mar. 2004.

[3] H. Wu, "Mathematical Modeling of Transient Transport Phenomena in PEM Fuel Cells."

[4] R. Ding, S. Zhang, Y. Chen, Z. Rui, K. Hua, Y. Wu, X. Li, X. Duan, X. Wang, J. Li, and J. Liu, "Application of Machine Learning in Optimizing Proton Exchange Membrane Fuel Cells: A Review," *Energy and AI*, vol. 9, p. 100170, Aug. 2022.

[5] L. Xu, Z. Hu, C. Fang, L. Xu, J. Li, and M. Ouyang, "A reduced-dimension dynamic model of a proton-exchange membrane fuel cell," *International Journal of Energy Research*, vol. 45, no. 12, pp. 18 002–18 017, Oct. 2021.

[6] E. Süli and D. F. Mayers, *An introduction to numerical analysis*. Cambridge university press, 2003.

[7] L. Fan, G. Zhang, and K. Jiao, "Characteristics of PEMFC operating at high current density with low external humidification," *Energy Conversion and Management*, vol. 150, pp. 763–774, Oct. 2017.

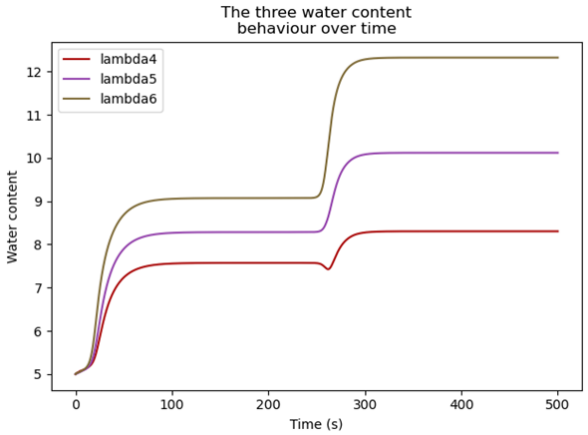

Fig. 4: Water content at three points of membrane versus time

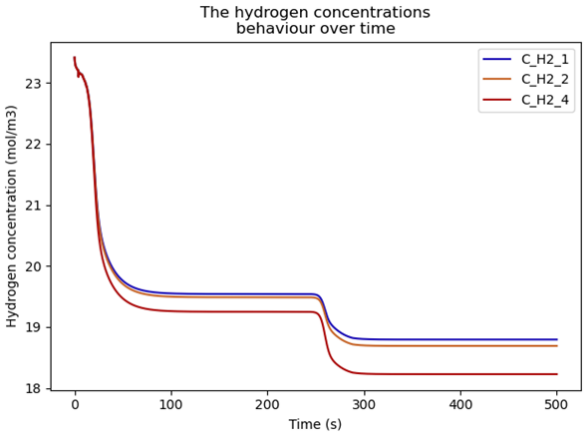

Fig. 7: Hydrogen concentration at anode side versus time

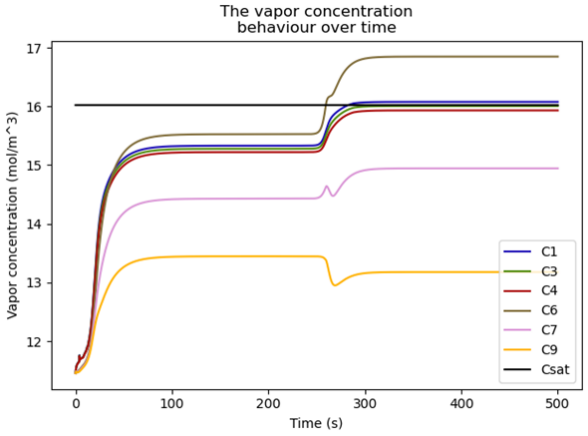

Fig. 5: Water concentration at different nodes versus time

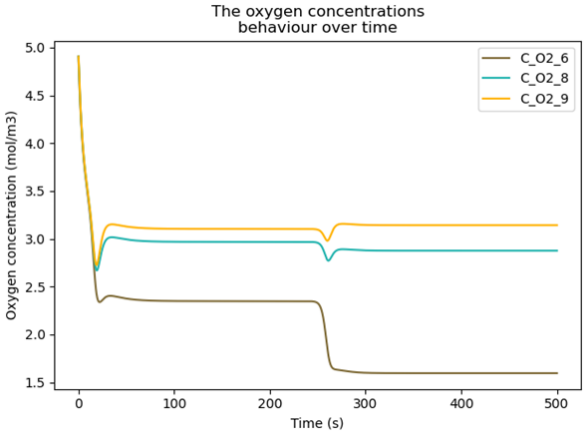

Fig. 8: Oxygen concentration at cathode side versus time

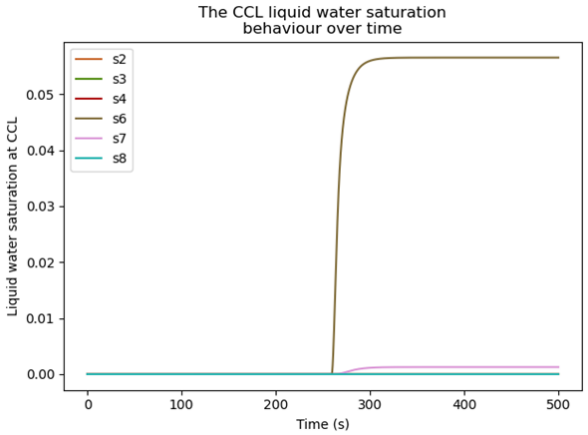

Fig. 6: Water saturation rate at CL and GDL versus time

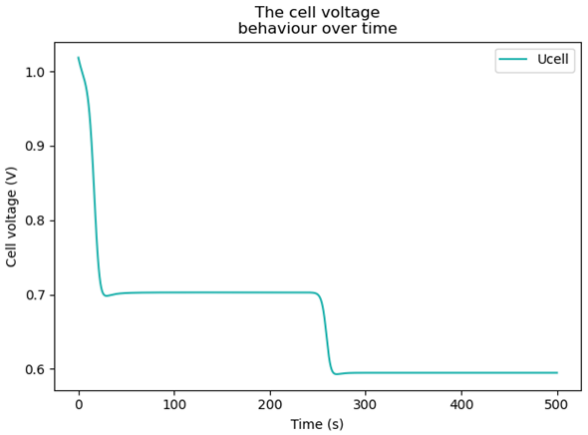

Fig. 9: Fuel cell voltage versus time